Virtually Bare Nanocrystal Surfaces: Significantly Enhanced Electrical Transport in $CuInSe_2$ and $CuIn_{1-x}Ga_xSe_2$ Thin Films upon Ligand Exchange with Thermally Degradable 1-Ethyl-5-Thiotetrazole

*Jannika Lauth, Jakob Marbach, Andreas Meyer, Sedat Dogan, Christian Klinke, Andreas Kornowski, and Horst Weller**

A facile and safe ligand exchange method for readily synthesized $CuInSe_2$ (CIS) and $CuIn_{1-x}Ga_xSe_2$ (CIGS) nanocrystals (NCs) from oleylamine to 1-ethyl-5-thiotetrazole, preserving the colloidal stability of the chalcopyrite structure, is presented. 1-Ethyl-5-thiotetrazole as thermally degradable ligand is adapted for the first time for trigonal pyramidal CIS (18 nm), elongated CIS (9 nm) and CIGS NCs (6 nm). Exchanged NC solutions are processed onto gold electrodes yielding ordered thin films. These films are thermally annealed at 260 °C to completely remove 1-ethyl-5-thiotetrazol leaving individual closely assembled NCs with virtually bare surfaces. The current–voltage characteristics of the NC solids are measured prior to ligand thermolysis in the dark and under illumination and after ligand thermolysis in the same manner. The conductivity of trigonal pyramidal CIS increases by four orders of magnitude (1.4×10^{-9} S cm^{-1} (dark) to 1.4×10^{-5} S cm^{-1} (illuminated)) for ligand-free NC films. Elongated CIS NC films show a three orders of magnitude conductivity increase and CIGS NC films exhibit improved conductivity by two orders of magnitude. Conductivity enhancement thereby depends on the NC size accentuating the role of trap-states and internal grain boundaries in ligand-free NC solids for electrical transport. This approach for the first time offers the possibility to address chalcopyrite materials' electrical properties in a virtually ligand-free state.

1. Introduction

Chalcopyrite materials, especially $CuInSe_2$ (CIS) and $CuIn_{1-x}Ga_xSe_2$ (CIGS) represent promising candidates for regenerative energy conversion. The direct band gap of 1.04 eV for pure CIS can be adjusted by the amount of gallium incorporated into the crystal lattice resulting in an increased band gap of up to 1.15 eV which is close to the optimum of best sun conversion efficiencies at AM1.5.[1,2] This tunability and the high absorption coefficient surpassing 10^5 cm^{-1} predestine the material for the use in solar cells.[3] A controlled stoichiometry of the system is thereby essential and can be for example sufficiently achieved by wet-chemical colloidal synthesis approaches for CIS and CIGS nanocrystals (NCs).[4,5] The significant progress of NC materials becomes apparent in their still emerging application in optoelectronics[4,6–11] including light emitting diodes (LEDs),[12,13] lasers,[14] and field effect transistors (FETs)[13,15] in the last two decades. Especially the solar cell sector is an important field that profits from ongoing focused research conducted in the NC sector, given the fact, that closely packed monolayers of PbS and CdSe quantum dots can enhance broad-band absorption via dipolar coupling[16] and multijunction quantum dot solar cells can significantly surpass the Shockley-Queisser limit.[17,18]

A crucial drawback still preventing most NC species from being accessible and profitable for electronic applications is the way they are processed. Wet-chemical approaches, on the one hand, represent low-cost ways to synthesize the material but, on the other hand, the obtained NCs are mostly stabilized with long-chained organic capping agents that secure stability in solution and prevent aggregation. At the same time, these organic surfactant molecules inhibit electronic interparticle interactions resulting in insulating behavior of NC assemblies.[13]

There are ways to increase the conductivity in NC solids for example by using inorganic metal chalcogenide complex ligands (MCCs)[19,20] but these involve the use of toxic and hazardous anhydrous hydrazine and are hard to apply in industrial large-scale dimensions. Chemical treatments with 1,2-ethanedithiol[21] and ethanethiol[22] show that photovoltaic device efficiency and electrical transport of NC films can be enhanced but ligand exchange is performed after the deposition of the

J. Lauth, J. Marbach, Dr. A. Meyer, S. Dogan, Prof. C. Klinke, A. Kornowski, Prof. H. Weller
Institute of Physical Chemistry
University of Hamburg
Grindelallee 117, D-20146, Hamburg, Germany
E-mail: horst.weller@chemie.uni-hamburg.de

DOI: 10.1002/adfm.201301957

© 2013 WILEY-VCH Verlag GmbH & Co. KGaA, Weinheim

NCs confining the flexibility of device fabrication. Further approaches like the use of thiocyanate as capping agent[23] and Meerwein's salt[24] for removing stabilizing amines, carboxylates and phosphonates have not yet been shown for CIS and CIGS. Recent results in stripping ligands off of NC surfaces with $(NH_4)_2S$[25] may be promising but have to show their abilities in determining the electrical transport properties of the NC materials.

Here, we report the characterization of two chalcopyrite NC systems CIS and CIGS with regard to their electrical transport properties once the initial oleylamine (OLA) ligand shell is exchanged by 1-ethyl-5-thiotetrazole (ETT). The capability of ETT as ligand and reactant for CdS NCs has been described by Voitekhovich et al.[26] Here, it is successfully implemented for the first time for CIS and CIGS NCs synthesized by modified methods of Panthani et al.[4] and Koo et al.[27] Our surfactant exchange method offers the possibility to control NC film thickness by the number of spin-coating steps. ETT as ligand represents a safe and straightforward opportunity to obtain highly conductive closely assembled organics-free CIS and CIGS NC solids that have great potential in photovoltaic applications.

2. Results and Discussion

2.1. Characterization of CIS and CIGS NCs

CIS and CIGS NCs were characterized using transmission electron microscopy (TEM), selected area electron diffraction (SAED), and powder X-ray diffraction (XRD). Trigonal pyramidal CIS NCs with an average size of 19 nm (±6 nm, edge length) were synthesized according to Koo et al.[27] (see Experimental Section for detailed syntheses and Supporting Information for XRD and SAED of the NCs). The TEM image in **Figure 1**a depicts the results of a typical ligand exchanged NC solution of trigonal pyramidal CIS. The crystal phase, structure and size distribution of the NCs remain unaltered after ligand exchange. (TEM images prior to ligand exchange, Figure S1 (Supporting Information), corresponding XRD and SAED, Figures S2,S3, Supporting Information). Elongated CIS NCs with an average size of 9 nm (±2 nm) and CIGS NCs with a mean diameter of 6 nm (±1 nm) were obtained by modifying a Panthani et al.[4] method and likewise ligand exchanged with ETT, see Figure 1b,c (TEM images prior to ligand exchange, Figure S4 (Supporting Information), (XRD and SAED, Figures S5,S6, Supporting Information) and Figure S7 (Supporting Information) (XRD and SAED, Figures S8,S9, Supporting Information).

Absorption spectra of CIS and CIGS NCs lack distinct excitonic absorption features (see Figure S10, Supporting Information). This phenomenon is well in accordance with observations made by Zhong et al.[28,29] and others[30,31] who attribute this behavior to the existence of inherent and surface traps in the NCs.

2.2. Ligand Exchange of CIS and CIGS NCs with ETT

2.2.1. Ligand Exchange Procedure

Ligand exchange of the NCs with ETT was conducted in solution. In a typical experiment 1 mL of a 0.025 M trigonal pyramidal CIS NC solution in chloroform, that had been precipitated once with 2-propanol, was mixed with 2 mL of a 2.8 M ETT chloroform solution (220 fold molar ligand excess, conditions for ligand exchange, see Table S1, Supporting Information). The ligand exchange mixture was stirred at 50 °C for 20 h (CIS NCs) respectively 30 h (CIGS NCs) and subsequently precipitated once with *n*-hexane. CIS and CIGS NCs maintained their size distribution and appearance (see Figure 1).

2.2.2. Attenuated Total Reflectance Fourier Transform Infrared Spectroscopy

Ligand exchange reactions were monitored using attenuated total Reflectance fourier transform infrared spectroscopy (ATR-FTIR). **Figure 2** shows IR spectra of initially OLA capped and ETT exchanged trigonal pyramidal CIS NCs (Δ-CIS). A well-known feature is the olefinic (–HC=CH–) stretching mode of the double bond in OLA at 3006 cm^{-1}.[32] This stretching mode is observable in the OLA stabilized sample and completely absent

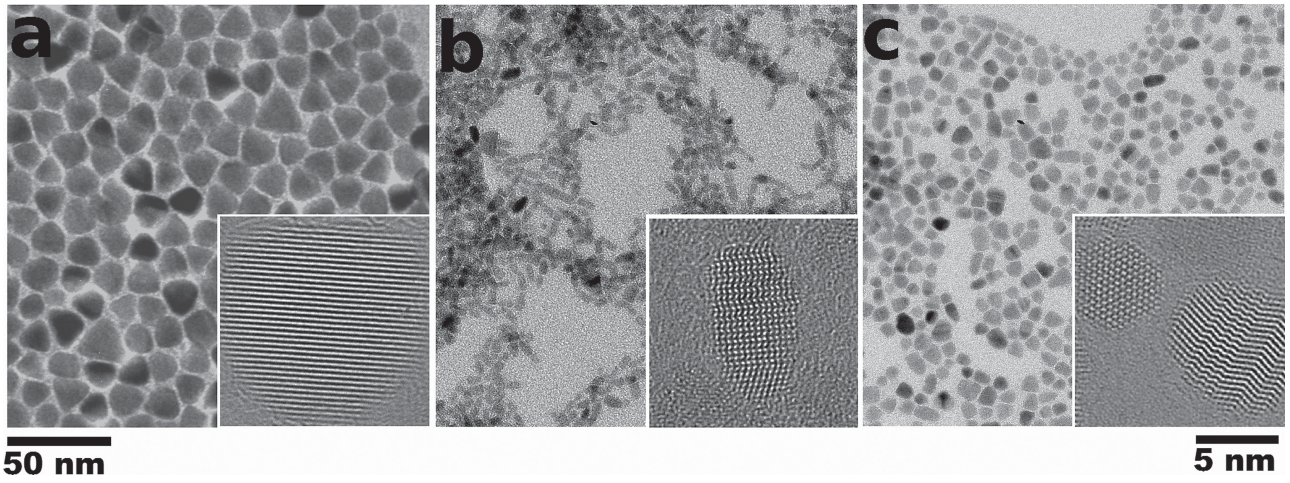

Figure 1. TEM images of ETT stabilized NCs, insets with single NCs a) trigonal pyramidal CIS, b) elongated CIS, and c) CIGS.

© 2013 WILEY-VCH Verlag GmbH & Co. KGaA, Weinheim

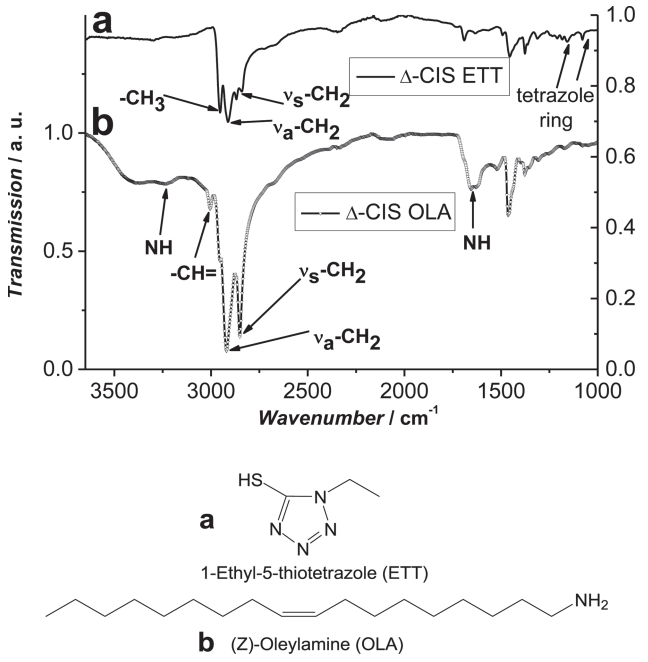

Figure 2. IR spectra of OLA capped and ETT exchanged NCs exemplarily shown for trigonal pyramidal NCs (Δ-CIS).

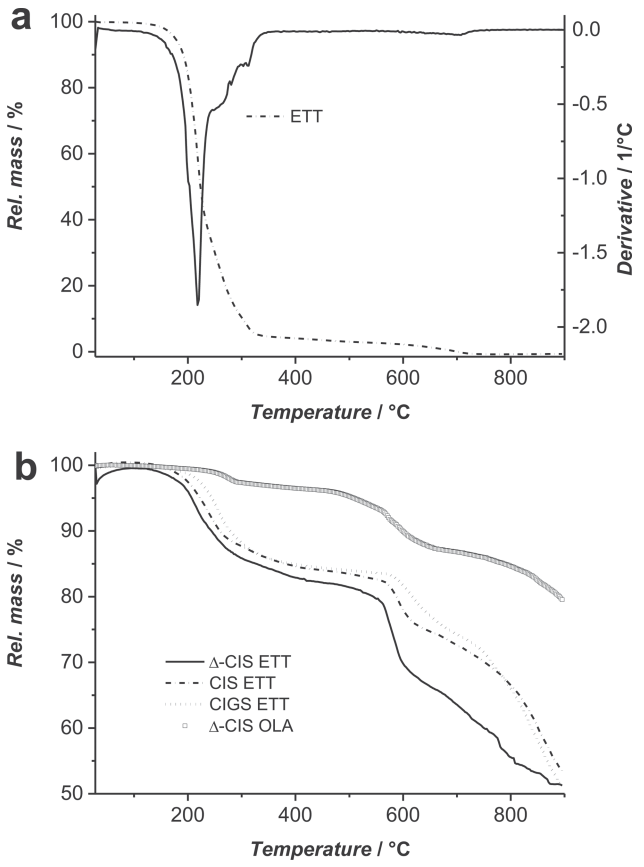

Figure 3. TGA of a) pure ETT with thermolysis temperature of 218 °C, b) ETT capped CIS and CIGS NCs and OLA capped trigonal pyramidal CIS NC sample for comparison, all ETT capped NCs show a distinct first mass loss attributed to ETT thermolysis in the range of 218–255 °C and a second mass loss originating from evaporating selenium at around 600 °C.

in all ETT stabilized NC samples (Figure 2 and Figure S11, Supporting Information). Distinct asymmetric and symmetric $–CH_2$ stretching vibrations of OLA occur near 2925 and 2850 cm^{-1} in OLA capped samples (Figure 2 and Figure S12, Supporting Information). After ETT exchange the $–CH_3$ vibration of the ethyl-group in ETT at 2950 cm^{-1} emerges. The $–CH_2$ vibration at 2850 cm^{-1} is still visible with lower intensity (only one $–CH_2$ group in ETT). OLA stabilized samples show broad N-H vibrations at 3250 cm^{-1} and 1650 cm^{-1} (Figure 2 and Figure S12, Supporting Information). These N–H vibrations are completely absent in ETT capped NC samples and confirm the assumption that ligand exchange of OLA by ETT was successful. ETT capped NCs show the weak stretching vibration of the tetrazole rings bound to the NC surface near 1020–1160 cm^{-1}.[33,34] As described by Voitekhovich et al.,[26] these vibrations tend to alter due to different binding possibilities of the tetrazole rings to the NC surface. Furthermore, in ETT capped NC samples the distinct vibration of the pure and unbound ligand at 3067 cm^{-1} is absent. This might be due to reduced vibration possibility of ETT when bound to a NC surface.

2.2.3. Thermogravimetric Analysis and Electron Ionization Mass Spectrometry

As ETT is known to decompose at moderate temperatures we followed the thermolysis of the ligand off NC surfaces by thermogravimetric analysis (TGA). NC samples were heated at a rate of 20 °C min^{-1} up to 550 °C under nitrogen flow and between 550 °C to 900 °C under a nitrogen/oxygen environment to remove residual carbon contents as carbon dioxide. **Figure 3**a shows the thermolysis of pure ETT with a single mass loss (94%) at 218 °C visible in the first derivative of the measurement and attributed to the decomposition of the ligand. At ≈700 °C remainders dissociate as volatile species under oxidative conditions (see Figure S13, Supporting Information, for first derivatives of ETT capped CIS and CIGS NCs). Figure 3b depicts that ETT capped CIS and CIGS NCs exhibit the same decomposition trend with a first mass loss attributed to ETT thermolysis between 218–255 °C. The second distinct mass loss occurring in all measurements at around 600 °C originates from selenium starting to evaporate from the samples at these temperatures. All ETT capped NCs undergo ligand thermolysis at lower temperatures than OLA capped NC samples (see Figure S14, Supporting Information).

Electron Ionization Mass Spectrometry (EI-MS) elucidates the decomposition way of ETT. With respect to a big fragment ion at m/z (%) 59 (68) [$HSCN^+$] originating from thiocyanic acid we can confirm the ring fragmentation reaction for cadmium 1-ethyl-5-thiotetrazole proposed by Voitekhovich et al.[26] An azide based decomposition of ETT is suggested as the spectrum lacks nitrogen associated mass peaks but shows fragment ions at m/z (%) 87 (8) [$HSCN_3^+$] as azide and sulfur containing part of the tetrazole ring and protonated azide at m/z (%) 43 (15) [HN_3^+].[35,36] Using the combined spectroscopic, thermogravimetric and spectrometric data we conclude

© 2013 WILEY-VCH Verlag GmbH & Co. KGaA, Weinheim

that ETT decomposes virtually completely under the described conditions leaving the surface of CIS and CIGS NCs organics-free with residual sulfur (EDS see Figures S15,S16, Supporting Information).

2.2.4. Small Angle X-Ray Scattering

To examine long-range ordering of ETT capped NCs in comparison with initial OLA capped samples small angle X-ray scattering (SAXS) measurements were performed. The use of spherical or cylindrical form factors and structure factors which represent the ordering of the NCs allow the precise determination of size and shape of the NCs, the interparticle distances and their size distribution. SAXS is an averaging method with results representing the full sample. SAXS results reveal that the interparticle distance of NCs decreases after ligand exchange from OLA to ETT and underpins the successful procedure. The center-to-center distance of elongated CIS NCs (size distribution determination: 5.6 nm ± 1.4 nm in length) decreases by 4.7 nm after ETT exchange (**Figure 4**a). This high value originates from the broad scattering profile and leads to certain inaccuracies in NC size distribution and in OLA length and spacing estimation (see simulated pattern). However, after ligand exchange ETT capped samples show significantly improved ordering visible in the narrowed peak width of the scattering curve and the fit quality of the associated simulated pattern. After heating the samples to 260 °C for 90 min the center-to-center distance of the ligand-free NC films further decreases by 0.6 nm. At the same time the peak width broadens due to close assembling and aggregation of the NCs in bare films.

The center-to-center distance of CIGS NCs (size distribution determination: 7.4 ± 1 nm) decreases by 0.9 nm after ligand exchange (Figure 4b). The peak width is significantly narrowed indicating small size distribution of the NCs and improved ordering. After annealing of the sample at 260 °C the center-to-center distance of the NCs further decreases by 0.7 nm and the peak width of the heated samples broadens like described for CIS NCs (see likewise TEM heating experiments, **Figure 5**, closely assembled individual CIGS NCs at 250 °C). SAXS patterns of trigonal pyramidal CIS NCs are excluded as the particles show a broad size distribution and lack distinct long-range ordering.

SAXS results show that elongated CIS and CIGS NCs both feature improved long range ordering after ligand exchange upon ETT accentuating the beneficial role of ETT as ligand for the chalcopyrite systems.

2.2.5. TEM Heating Experiments

To trace the exact processes during the NC thin film annealing step and the coalescence of the NCs at temperatures exceeding 260 °C we performed stepwise heating of ETT capped CIGS NCs inside the TEM. At every heating equilibration step EDS was performed (see Figures S15,S16, Supporting Information, for zoom in). The materials' composition and chalcopyrite crystal phase thereby stay unaltered in the temperature range up to 400 °C also seen in the SAED of the sample (Figure S17, Supporting Information). Figure 5 shows CIGS NCs at different temperatures. A reduced interparticle distance as determined

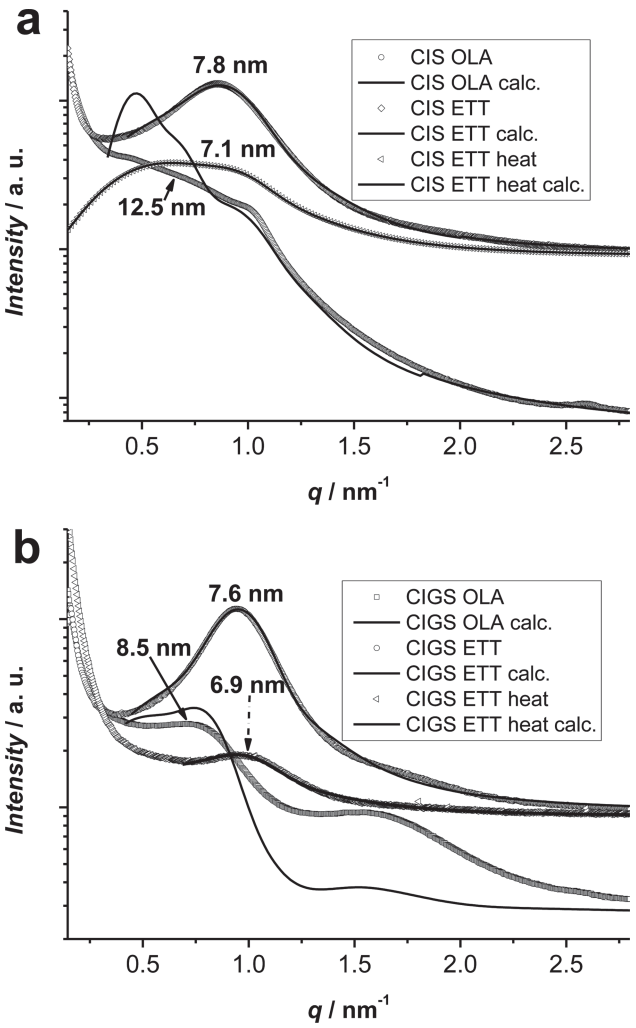

Figure 4. SAXS of a) elongated CIS NCs, showing reduced center-to-center distance and improved ordering of NCs after ETT exchange b) CIGS NCs prior to and after ligand exchange, center-to-center distance decreases from OLA capped over ETT exchanged to heated and ligand-free NCs, ordering improves after ligand exchange and decreases after heating of the sample.

by SAXS is also apparent in the TEM images at 250 °C, the temperature where ETT starts to decompose. At 400 °C the NCs have started sintering and form assemblies. During heating of the CIGS NCs residual sulfur from ETT exchange is completely removed within the heating range (see Figure S16, Supporting Information, zoom in).

Comprehensive analysis of the ligand exchange processes of CIS and CIGS NCs with ETT including ATR-FTIR, TGA, SAXS, and TEM heating experiments emphasize the successful functionalization of the materials. ATR-FTIR measurements and TGA underpin the complete ligand exchange. SAXS measurements reveal that after ligand exchange interparticle distances are reduced and improved long-range ordering of elongated CIS and CIGS is apparent. Heating experiments inside TEM show that after thermolysis of ETT sintering of virtually bare-surfaced and organics-free CIGS NCs is possible at around

© 2013 WILEY-VCH Verlag GmbH & Co. KGaA, Weinheim

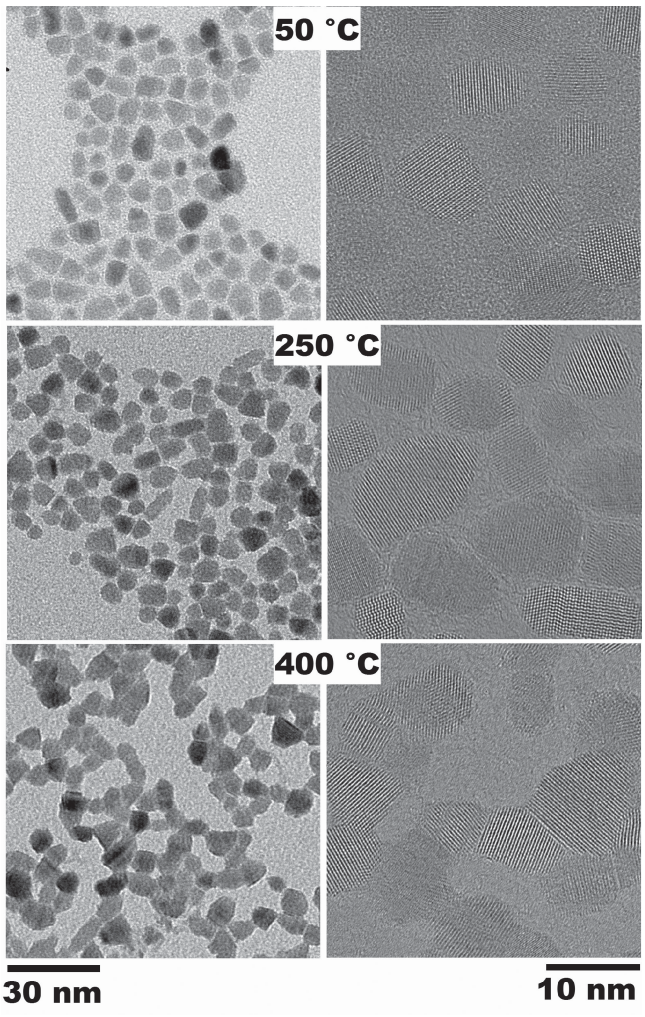

Figure 5. Heating experiment of CIGS NCs inside TEM at 50 °C, 250 °C with reduced interparticle spacing, at 400 °C NCs have started sintering.

400 °C without altering the chalcopyrite crystal phase and stoichiometry of the material.

2.3. Electrical Transport Measurements

Electrical transport in closely assembled NC solids is highly dependent on NC surface functionalization. Long-chained organic capping agents like OLA suppress effective interparticle coupling and lead to high tunnelling barriers for electrons and thus insulating behavior of the materials.[13] Reduced interparticle distance improves particle coupling and hence charge transport in NC assemblies. To monitor the effect of reduced interparticle spacing upon ETT exchange, we investigate the electrical transport behavior of the CI(G)S NCs before and after ETT thermolysis. The current–voltage characteristics of trigonal pyramidal and elongated CIS thin films as well as CIGS thin films are measured in the dark and under illumination. As ETT undergoes thermolysis at different temperatures for the three systems (see Figure 3b and Figure S13, Supporting Information) all NC thin film samples were heated to 260 °C to assure complete ETT decomposition and comparable conditions but prevent sintering of the NCs as observed at 400 °C. In a typical experiment 20 µL (2 × 10 µL) of a colloidal CI(G)S NC solution were spin-coated (20 s at 500 rpm, subsequently 20 s at 2000 rpm) onto a highly n-doped silicon substrate with a 300 nm insulating layer of silicon oxide and pre-deposited gold electrodes. Directly after spin-coating the substrates were transferred to a probe station connected with a parameter analyzer and electrical measurements were carried out under vacuum conditions. The NC thin films are characterized in the dark and under illumination with a Schott ACE 150 Watt halogen AC powered light source with fiber optics. The bias voltage V_{ds} is swept between –5 V and +5 V. After measuring the current–voltage curves of ETT capped NCs the samples were transferred to an oven and heated to 260 °C for 90 min under oil pump vacuum. The annealed samples were kept under argon as they were prone to oxidation and transferred back to the probe station. The previously characterized devices are measured again in the dark and under illumination. The conductivity (σ) of the samples is then calculated according to

$$\sigma = \frac{I_{ds}}{V_{ds}} \frac{L}{hW} \quad (1)$$

with V_{ds} = +200 mV, channel length L = 300 nm for trigonal pyramidal CIS, 350 nm for elongated CIS and CIGS, width W = 14.5 µm, and height h of the film ≈20 nm for trigonal pyramidal CIS and ≈40 nm for elongated CIS and CIGS films. I_{ds} is the current detected at every measured value. NC thin films which were exemplarily heated to 400 °C to enable sintering of the NCs were excluded from current–voltage measurements as they featured intercalation of the NCs into the electrode setup. Different electrode settings are under investigation to address this problem. **Figure 6**a shows the current–voltage characteristics of a trigonal pyramidal NC thin film before and after ETT thermolysis on the logarithmic scale (Figure S18–S20, Supporting Information, for high resolution SEM images of the NC thin films showing no sintering processes).

Table 1 shows the calculated conductivities of ETT capped CIS and CIGS NCs. Prior to ligand thermolysis trigonal pyramidal CIS NC exhibit a conductivity of 1.4×10^{-9} S cm^{-1} in the dark. These values are comparable to conductivities exemplarily measured for trigonal pyramidal CIS NCs capped with the initial ligand OLA under same conditions. After ETT thermolysis however the NC film shows a significant four orders of magnitude enhanced electrical transport with a conductivity of 1.4×10^{-5} S cm^{-1} under illumination. Elongated CIS NC films were characterized likewise (see Table 1 and Figure 6b) exhibiting conductivities of 3.7×10^{-9} S cm^{-1} in the dark prior to ligand thermolysis. The hysteresis in the current–voltage curves of ETT capped samples prior to heating (Figure 6a–c) originates from charging of the NC film when a bias voltage of –5 V to +5 V is applied. However, after annealing this effect is minimized once more underpinning the successful ligand-free state of the NC films. Electrical transport in elongated ligand-free CIS NCs is enhanced by three orders of magnitude to conductivities of 6.8×10^{-6} S cm^{-1} under illumination. In comparison with trigonal pyramidal NCs it is apparent that the NC size plays a crucial role in electrical transport of the CIS materials.

© 2013 WILEY-VCH Verlag GmbH & Co. KGaA, Weinheim

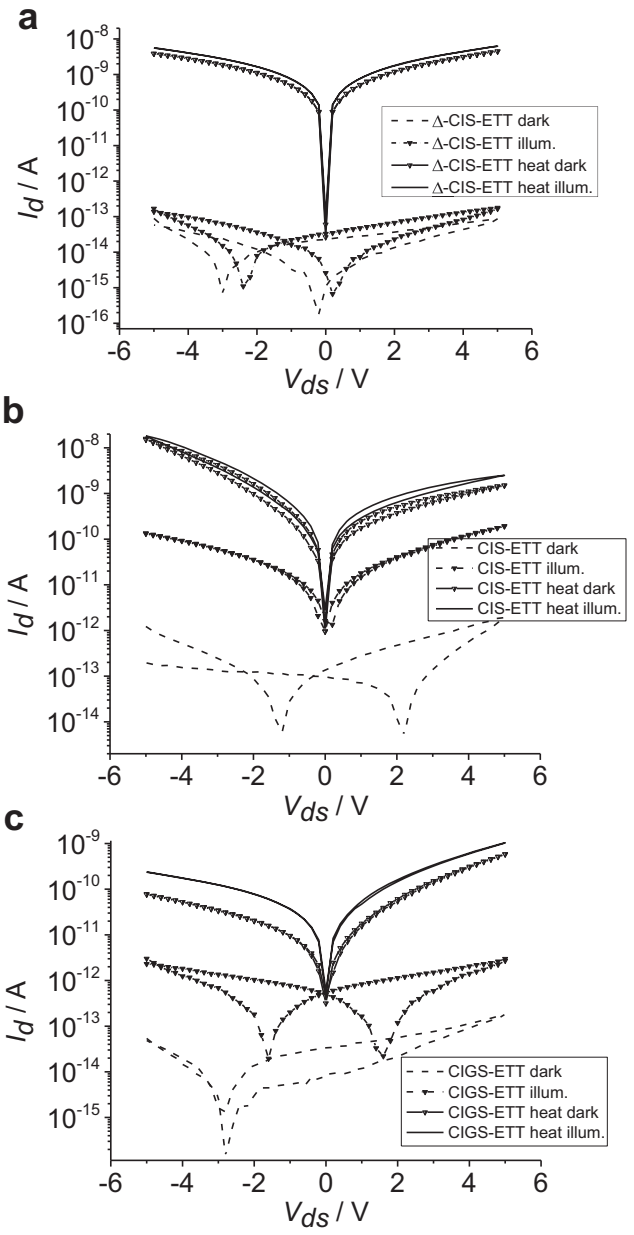

Figure 6. Current–voltage curves at room temperature: a) trigonal pyramidal CIS NCs (Δ-CIS), conductivity increase by four orders of magnitude after thermolysis of ETT, b) elongated CIS NCs and three orders of magnitude enhancement in conductivity after ETT thermolysis under illumination compared to conductivity in the dark prior to ETT thermolysis, c) CIGS NCs, conductivity improvement by two orders of magnitude in total.

Table 1. Conductivity of CIS and CIGS NCs.

	Trigonal pyramidal CIS σ [S cm^{-1}]	Elongated CIS σ [S cm^{-1}]	CIGS σ [S cm^{-1}]
ETT dark	1.4×10^{-9}	3.7×10^{-9}	1.0×10^{-9}
ETT illuminated	4.0×10^{-9}	6.8×10^{-8}	1.3×10^{-8}
ETT heat dark	7.5×10^{-6}	8.2×10^{-7}	6.0×10^{-8}
ETT heat illuminated	1.4×10^{-5}	6.8×10^{-6}	1.9×10^{-7}

Elongated CIS NCs with an average size of 9 nm show 1.5 orders of magnitude reduced conductivity compared to 19 nm sized trigonal pyramidal CIS NCs. Two factors are supposable for this behavior: 1) The higher surface-to-volume ratio in smaller and organic ligand-free NCs leads to more surface originating trapping states known to reduce electrical transport.[37] 2) Charge carriers in smaller NCs have to overcome more grain boundaries to cross the channel length and will likely more often recombine.

Figure 6c shows electrical transport of spherical CIGS NC films exhibiting conductivities of 1.0×10^{-9} S cm^{-1} in the dark prior to ligand thermolysis. After annealing the same devices show two orders of magnitude enhanced conductivity of 1.9×10^{-7} S cm^{-1} under illumination. Here again the higher number of trap states and grain boundaries in smaller NCs may lead to a lower conductivity. All NC types show photoresponse after ligand thermolysis whereas CIGS NCs exhibit the strongest effect. The current measured at +5 V increases from 5×10^{-10} to 1×10^{-9} Ampere, a two-fold gain, when ligand-free NCs are illuminated by diffuse microscope light (see Figure S21C, Supporting Information).

3. Conclusion

We have demonstrated the successful functionalization of CIS and CIGS NCs with ETT as thermally degradable ligand preserving the NC's colloidal stability prior to ligand thermolysis and obtaining closely assembled organics-free individual NCs after the annealing step. By this straight forward, facile, and safe method for the first time we investigated CIS and CIGS NC solids' significantly enhanced electrical transport in a virtually ligand-free state. Additionally ETT exchanged NCs can be sintered to form close crystalline assemblies without altering the chalcopyrite crystal structure and composition of the material.

The combination of synthesis, detailed characterization and application of the chalcopyrites yields CIS and CIGS NC materials that hold high potential for the utilization in photovoltaic devices.

4. Experimental Section

Chemicals: All Chemicals were used as received without further purification. Copper(I) acetate (Cu(OAc), STREM, 99%), copper(I) chloride (CuCl, Sigma Aldrich, 99.995%), indium(III) chloride ($InCl_3$, Sigma Aldrich, 99.99%), gallium(III) iodide (GaI_3, Sigma Aldrich, 99.999%), selenourea (Sigma Aldrich, 98%), and oleylamine (OLA, Acros Organics, 80–90%) were stored in a glovebox in a nitrogen environment. Trioctylphosphine (TOP, 90%) was purchased from Sigma Aldrich and stored under ambient conditions.

Methods: Unless stated otherwise all synthetic steps were carried out using standard Schlenk-line techniques under nitrogen as inert gas or inside a nitrogen filled glovebox.

Synthesis of Trigonal Pyramidal $CuInSe_2$: Trigonal pyramidal $CuInSe_2$ NCs were synthesized according to a method of Koo et al.[27] In a typical synthesis of 19 nm NCs 0.50 mmol (50 mg) copper(I) chloride were mixed with 0.500 mmol (111 mg) indium(III) chloride inside a glovebox in a 25 mL three-neck flask equipped with a septum and thermocouple. 10 mL OLA were added to the components and the solution marked A. The flask was connected to a condenser under nitrogen flow outside of the glovebox. In a separate 5 mL three-neck flask likewise equipped with septum, thermocouple and condenser, 1.00 mmol (123 mg) selenourea

© 2013 WILEY-VCH Verlag GmbH & Co. KGaA, Weinheim

was mixed with 1 mL OLA and marked solution B. Solution A was kept stirring under oil pump vacuum at 60 °C for one hour and solution B was stirred under nitrogen flow. After one hour solution A was set under nitrogen, heated to 130 °C for 10 min and subsequently cooled to 100 °C. Solution B meanwhile was heated to 210 °C to dissolve the reactant and set free reactive selenium species for reaction. Subsequently, it was cooled to 110 °C, taken out by syringe and rapidly injected into solution A. The reaction mixture was then heated to 240 °C at a rate of 15 °C min^{-1}. After one hour of reaction time the suspension was cooled to room temperature. 30 mL of ethanol were added to the crude product to precipitate the NCs. The mixture was centrifuged at 4000 rpm for 4 min. The colorless supernatant was discarded and the NCs redissolved in 5 mL chloroform. After centrifugation of this solution at 4000 rpm for 5 min the NC product in the deep black supernatant was separated from the sediment which contained poorly capped NCs. The reaction typically yielded ≈50% purified NCs. Characterization and ligand exchange was conducted with the purified NCs from the supernatant (Figure S1–S3, Supporting Information).

Synthesis of Elongated $CuInSe_2$: Elongated $CuInSe_2$ NCs were synthesized based on a method by Panthani et al.[4] A typical synthesis included 0.50 mmol (61 mg) copper(I) acetate, 0.500 mmol (111 mg) indium(III) chloride and 1.00 mmol (123 mg) selenourea mixed in a 25 mL three-neck flask and combined with 10 mL OLA. The reaction solution was kept under oil pump vacuum at 60 °C for one hour, then set under nitrogen and stirred for another hour at 110 °C. Subsequently the mixture was heated to 240 °C and kept at this temperature for one hour. Afterwards, the solution was cooled to room temperature. For purification and better stabilization of the NC product 4 mL of a TOP/toluene mixture (TOP/Tol 3:1) was added to the crude product. The solution was vortexed and centrifuged at 4500 rpm for 5 min to remove poorly capped NCs. The supernatant was separated from the sediment and 30 mL 2-propanol was added for precipitation. The mixture was centrifuged at 10000 rpm for 15 min. The NC product was redissolved in 5 mL chloroform and filtrated with a 0.2 µm hydrophobic syringe filter. 15 mL of a methanol/2-propanol solution (4:1) were added and the mixture centrifuged at 10000 rpm for 5 min. The reaction typically yielded ≈25% (Figure S4–S6, Supporting Information). NCs were redissolved in chloroform and used for characterization and ligand exchange.

Synthesis of $CuIn_{1-x}Ga_xSe_2$: $CuIn_{1-x}Ga_xSe_2$ NCs were synthesized based on a method by Panthani et al.[4] In a typical one-pot synthesis 0.10 mmol (12 mg) copper(I) acetate, 0.10 mmol (22 mg) indium(III) chloride, 0.10 mmol (45 mg) gallium(III) iodide, and 0.20 mmol (25 mg) selenourea were mixed in a 25 mL three-neck flask and 10 mL OLA were added. The reaction mixture was stirred at 60 °C under oil pump vacuum, then set under nitrogen and stirred at 110 °C for an additional hour and subsequently heated to 240 °C and kept at that temperature for one hour for reaction. Afterwards the solution was allowed to cool to room temperature. For purification and better stabilization of the NC product 4 mL of TOP/Tol (3:1) were added to the crude product. The solution was vortexed and centrifuged at 5600 rpm for 5 min to remove poorly capped NCs. The supernatant was separated and 25 mL 2-propanol were added for precipitation. The mixture was centrifuged at 10000 rpm for 15 min. The NCs were redissolved in 2 mL chloroform and filtrated with a 0.2 µm hydrophobic syringe filter. The reaction typically yielded ≈60% (Figure S7–S9, Supporting Information).

1-Ethyl-5-thiotetrazole: 1-Ethyl-5-thiotetrazole was synthesized by cycloaddition of sodium azide to ethyl isothiocyanate according to well established literature procedures.[38,39]

Transmission Electron Microscopy: TEM imaging was conducted either with a JEOL JEM 2200FS (UHR) with CESCOR and CETCOR corrector at an acceleration voltage of 200 kV, a Philips CM 300 UT at an acceleration voltage of 200 kV or a JEOL JEM 1011 microscope at 100 kV equipped with a CCD camera.

Energy Dispersive X-Ray Spectroscopy: Quantitative elemental analysis of NCs was obtained using a Si(Li) JEOL JED-2300 energy dispersive X-ray detector installed at the JEOL JEM 2200FS or with an EDAX DX-4 system installed at the Philips CM 300 UT.

Scanning Electron Microscopy: SEM images were obtained on a LEO1550 scanning electron microscope with a spatial resolution of ≈1 nm.

X-Ray Diffraction: Powder XRDs were recorded using a Philipps X'Pert-diffractometer with Bragg-Brentano-geometry on applying copper-Kα radiation.

Attenuated Total Reflectance Fourier Transform Infrared Spectroscopy (ATR-FTIR): IR spectra were recorded with a *Bruker Equinox 55* ATR-FTIR technique. The dried NC sample was placed on the crystal of the ATR unit and the spectra recorded in the range of 600–4000 cm^{-1}.

Small Angle X-Ray Scattering: SAXS experiments were performed at a rotating anode device consisting of a rotating copper (Cu) anode (Seifert, Ahrensburg), crossed Goebel mirrors, and an image plate detector (Fuji) at a sample–detector distance of 1.0 m. The revealed scattering patterns were radially integrated, transformed into SAXS curves and analyzed with the software Scatter.[40] Scatter is an application for analyzing small angle X-ray scattering (SAXS) and Small Angle Neutron Scattering (SANS) curves and patterns of nano- and mesoscopically structured materials.

Thermogravimetric Analysis: TGA studies were carried out using a *Netzsch TG 209 C* in the temperature range of 25–550 °C with a heating rate of 20 °C min^{-1} under nitrogen atmosphere. Subsequently samples were heated from 550–900 °C under oxygen/nitrogen atmosphere at a rate of 20 °C min^{-1}.

Characterization of Electrical Transport and Conductivity Measurements: Electrical measurements were performed on a 4200-SCS semiconductor characterization system from Keithley Instruments inside a VFTTP4 probe station by Lake Shore Cryotronics.

Supporting Information

Supporting Information is available from the Wiley Online Library or from the author.

Acknowledgements

The authors gratefully acknowledge Jan Michels for the possibility to use the Atomic Layer Deposition system of the Bachmann group for heating of the NC coated Si/SiO_2 substrates. Carsten Ott from the Center for Applied Nanotechnology (CAN) Company in Hamburg, Germany is gratefully acknowledged for synthesizing and providing the 1-ethyl-5-thiotetrazole (ETT) ligand.

Received: June 7, 2013
Revised: July 31, 2013
Published online: September 23, 2013

[1] F. Hergert, S. Jost, R. Hock, M. Purwins, *J. Solid State Chem.* **2006**, *179*, 2394.
[2] W. Shockley, H. J. Queisser, *J. Appl. Phys.* **1961**, *32*, 510.
[3] B. J. Stanbery, *Crit. Rev. Solid State Mater. Sci.* **2002**, *27*, 73.
[4] M. G. Panthani, V. Akhavan, B. Goodfellow, J. P. Schmidtke, L. Dunn, A. Dodabalapur, P. F. Barbara, B. A. Korgel, *J. Am. Chem. Soc.* **2008**, *130*, 16770.
[5] J. Tang, S. Hinds, S. O. Kelley, E. H. Sargent, *Chem. Mater.* **2008**, *20*, 6906.
[6] V. A. Akhavan, M. G. Panthani, B. W. Goodfellow, D. K. Reid, B. A. Korgel, *Opt. Express* **2010**, *18*, A411.
[7] Q. Guo, S. J. Kim, M. Kar, W. N. Shafarman, R. W. Birkmire, E. A. Stach, R. Agrawal, H. W. Hillhouse, *Nano Lett.* **2008**, *8*, 2982.
[8] I. Gur, N. A. Fromer, M. L. Geier, A. P. Alivisatos, *Science* **2005**, *310*, 462.

© 2013 WILEY-VCH Verlag GmbH & Co. KGaA, Weinheim

[9] K. W. Johnston, A. G. Pattantyus-Abraham, J. P. Clifford, S. H. Myrskog, D. D. MacNeil, L. Levina, E. H. Sargent, *Appl. Phys. Lett.* **2008**, *92*, 151115.
[10] F. Shen, W. Que, P. Zhong, J. Zhang, X. Yin, *Coll. Surf. A: Physicochem. Eng. Asp.* **2011**, *392*, 1.
[11] Y. Yang, H. Zhong, Z. Bai, B. Zou, Y. Li, G. D. Scholes, *J. Phys. Chem. C* **2012**, *116*, 7280.
[12] C. B. Murray, C. R. Kagan, M. G. Bawendi, *Ann. Rev. Mater. Sci.* **2000**, *30*, 545.
[13] D. V. Talapin, J.-S. Lee, M. V. Kovalenko, E. V. Shevchenko, *Chem. Rev.* **2010**, *110*, 389.
[14] V. I. Klimov, A. A. Mikhailovsky, S. Xu, A. Malko, J. A. Hollingsworth, C. A. Leatherdale, H.-J. Eisler, M. G. Bawendi, *Science* **2000**, *290*, 314.
[15] D. V. Talapin, C. B. Murray, *Science* **2005**, *310*, 86.
[16] P. Geiregat, Y. Justo, S. Abe, S. Flamee, Z. Hens, *ACS Nano* **2013**, *7*, 987.
[17] M. C. Beard, J. M. Luther, O. E. Semonin, A. J. Nozik, *Acc. Chem. Res.* **2013**, *46*, 1252.
[18] O. E. Semonin, J. M. Luther, S. Choi, H.-Y. Chen, J. Gao, A. J. Nozik, M. C. Beard, *Science* **2011**, *334*, 1530.
[19] A. de Kergommeaux, A. Fiore, J. Faure-Vincent, F. Chandezon, A. Pron, R. de Bettignies, P. Reiss, *Mater. Chem. Phys.* **2012**, *136*, 877.
[20] M. V. Kovalenko, M. Scheele, D. V. Talapin, *Science* **2009**, *324*, 1417.
[21] J. M. Luther, M. Law, Q. Song, C. L. Perkins, M. C. Beard, A. J. Nozik, *ACS Nano* **2008**, *2*, 271.
[22] D. A. R. Barkhouse, A. G. Pattantyus-Abraham, L. Levina, E. H. Sargent, *ACS Nano* **2008**, *2*, 2356.
[23] A. T. Fafarman, W. Koh, B. T. Diroll, D. K. Kim, D.-K. Ko, S. J. Oh, X. Ye, V. Doan-Nguyen, M. R. Crump, D. C. Reifsnyder, C. B. Murray, C. R. Kagan, *J. Am. Chem. Soc.* **2011**, *133*, 15753.
[24] E. L. Rosen, R. Buonsanti, A. Llordes, A. M. Sawvel, D. J. Milliron, B. A. Helms, *Angew. Chem. Int. Ed.* **2012**, *51*, 684.
[25] H. Zhang, B. Hu, L. Sun, R. Hovden, F. W. Wise, D. A. Muller, R. D. Robinson, *Nano Lett.* **2011**, *11*, 5356.
[26] S. V. Voitekhovich, D. V. Talapin, C. Klinke, A. Kornowski, H. Weller, *Chem. Mater.* **2008**, *20*, 4545.
[27] B. Koo, R. N. Patel, B. A. Korgel, *J. Am. Chem. Soc.* **2009**, *131*, 3134.
[28] H. Zhong, Y. Li, M. Ye, Z. Zhu, Y. Zhou, C. Yang, Y. Li, *Nanotechnology* **2007**, *18*, 025602.
[29] H. Zhong, Z. Wang, E. Bovero, Z. Lu, F. C. J. M. van Veggel, G. D. Scholes, *J. Phys. Chem. C* **2011**, *115*, 12396.
[30] P. M. Allen, M. G. Bawendi, *J. Am. Chem. Soc.* **2008**, *130*, 9240.
[31] K. Nose, T. Omata, S. Otsuka-Yao-Matsuo, *J. Phys. Chem. C* **2009**, *113*, 3455.
[32] N. Shukla, E. B. Svedberg, J. Ell, *Coll. Surf. A: Physicochem. Eng. Asp.* **2007**, *301*, 113.
[33] A. Gómez-Zavaglia, I. D. Reva, L. Frija, M. L. Cristiano, R. Fausto, *J. Mol. Struct.* **2006**, *786*, 182.
[34] B. Sägmüller, P. Freunscht, S. Schneider, *J. Mol. Struct.* **1999**, *482*, 231.
[35] K. W. Paul, M. M. Hurley, K. K. Irikura, *J. Phys. Chem. A* **2009**, *113*, 2483.
[36] N. Piekiel, M. R. Zachariah, *J. Phys. Chem. A* **2012**, *116*, 1519.
[37] P. Nagpal, V. I. Klimov, *Nat. Commun.* **2011**, *2*, 486.
[38] P. J. Kocienski, A. Bell, P. R. Blakemore, *Synlett* **2000**, *2000*, 365.
[39] H. R. Meier, H. Heimgartner, *Methoden der Organischen Chemie (Houben-Weyl)*, Vol. *8*, (Ed: E. Schumann), Georg Thieme, Stuttgart, Germany **1994**, p 664.
[40] S. Förster, L. Apostol, W. Bras, *J. Appl. Cryst.* **2010**, *43*, 639.

© 2013 WILEY-VCH Verlag GmbH & Co. KGaA, Weinheim